DOI: https://doi.org/10.15276/hait.09.2026.44
UDC 629.113.65:621.313.3:519.87.004

In-wheel surface-mounted permanent magnet motor design for light electric vehicle based on drive cycle WLTC Class 1

Ihor Z. Shchur[1)]
ORCID: https://orcid.org/0000-0001-7346-1463; ihor.z.shchur@lpnu.ua. Scopus Author ID: 36348908300
Ihor Y. Lutchyn[1)]
ORCID: https://orcid.org/0009-0003-2691-9381; ihor.y.lutchyn@lpnu.ua. Scopus Author ID: 60560224000
Marek Lis[2)]
ORCID: https://orcid.org/0000-0001-5191-8303; marek.lis@pcz.pl. Scopus Author ID: 54415858000
[1)] Lviv Polytechnic National University, 12, Stepana Bandery Str. Lviv, Ukraine
[2)] Czestochowa University of Technology, 17, Al. Armii Krajowej. Czestohowa, Poland

ABSTRACT

Relevance: For designing traction electric motors, the approach focused on the motor operation at the rated mode point traditionally dominates. However, electric vehicle motors constantly operate in a wide range of torque and angular velocity changes. Accordingly, it is advisable to design an electric machine so that the zone of its optimal operation (maximum efficiency) is located in the area where the motor operates for the most time in the drive cycle. A literature review shows that such an approach makes it possible to increase the efficiency of the traction motor and with it the overall efficiency of the electric drive system. **The purpose** of this article is to develop an in-wheel traction surface-mounted permanent magnet synchronous motor (SPMSM) for a light electric vehicle – a high-speed electric bicycle – based on the new drive cycle WLTC Class 1 for light electric vehicle. **Methods**: For this purpose, a histogram of the combination of angular velocity and torque was obtained for the light electric vehicle under study while executing the specified drive cycle. According to the determined from the histogram range where the drive operates most often, the parameters of the experimental SPMSM were determined, moreover, for its operation in two regions of angular velocity control – with constant torque and constant power. In the MATLAB/Simulink environment, an SPMSM model was built taking into account copper and core losses, based on which the operational efficiency of the experimental (with two region of angular velocity regulation) and typical (with single region of angular velocity regulation) SPMSMs were studied. These studies provided information for the construction efficiency maps of these motors in the Surfer environment. A comparison of the operational efficiency of the light electric vehicle under study in the drive cycle, separately with the experimental and typical motors, was carried out by modeling in the MATLAB/Simulink environment using the Energetic Macroscopic Representation (EMR) method. **The results** of the study showed a decrease in electricity consumption for the execution of the drive cycle by the light electric vehicle with the experimental SPMSM by 2.37 %, as well as an increase in regenerative braking energy by 3.62 % compared to the typical motor. **Conclusions**: The results obtained confirm the effectiveness of the decisions made – SPMSM with two-region angular velocity regulation and the correspondingly obtained based parameters makes it possible to halve its rated power and simultaneously increase the overall efficiency of the electric bicycle drive system.

Keywords: Light electric vehicle (LEV), WLTC Class 1 drive cycle, surface-mounted permanent magnet synchronous motor (SPMSM), two-region angular velocity regulation, energy efficiency map, Energetic Macroscopic Representation (EMR)

***For citation*: Shchur I. Z., Lutchyn I. Y., Lis M. "In-wheel surface-mounted permanent magnet motor design for light electric vehicle based on drive cycle WLTC Class 1". *Herald of Advanced Information Technology*. 2026; Vol.9 No.4: 718–735. DOI: https://doi.org/10.15276/hait.09.2026.44**

1. INTRODUCTION

Electric vehicles (EVs) are rapidly and irreversibly replacing environmentally problematic, structurally more complex, and significantly more expensive-to-operate traditional internal combustion engine vehicles. However, to accelerate this transition, it is still necessary to solve a number of problems related to increasing the specific energy of batteries, increasing the EV range and creating a dense network of charging stations [1]. From the perspective of EV design, the relationship between the vehicle mass, the required battery capacity, the traction drive power and the range is particularly cing the mass of the EV reduces the required traction important. Reduеffort, which, in turn, allows using of a battery and an electric motor of lower power and mass. At the same time, for EVs, it is advisable to consider not the maximum power of the traction motor as a self-sufficient criterion, but the correspondence of its characteristics to the real vehicle movement profile.

Among all EVs, a separate promising category of urban mobility has recently emerged – Light Electric Vehicles (LEV) [2]. LEVs include, in particular, electric bicycles, electric scooters, electric one- and two-wheeled vehicles, which allow for more efficient use of urban space for transport. The advantages of LEVs should be assessed comprehensively – through efficiency, resource

© Shchur I., Lutchyn I., Lis Marek, 2026

This is an open access article under the CC BY license (https://creativecommons.org/licenses/by/4.0/deed.uk)

ISSN 2663-0176 (Print)
ISSN 2663-7731 (Online)

consumption, transport functionality and impact on the urban environment [3]. With this in mind, when designing a LEV traction system, the power, mass, and efficiency of the electric drive should be aligned with the operating characteristics of a particular vehicle [4].

2. LITERATURE REVIEW AND PROBLEM STATEMENT

A promising solution for LEV is to integrate the traction electric motor directly into the wheel. Direct-drive in-wheel motor (IWM) allows to eliminate the gearbox, differential and other elements of mechanical transmission simplifying the structure of the electric drive and reducing mechanical losses [5].

A comparative analysis of induction motors and synchronous machines with permanent magnets (PM), including those placed on the rotor surface surface-mounted permanent magnet synchronous motor (SPMSM) and formed inside the rotor (IPMSM) [6], shows that, for direct-drive IWM, SPMSM is the most suitable due to its simplicity of design and control, as well as high efficiency, although it is inferior to IPMSM in terms of its ability to operate in a wide high-speed region. For LEVs with a relatively low maximum speed, this disadvantage is less critical, while the SPMSM design is much simpler and cheaper that well meets the requirements for mass production and availability of such EVs. The simplest implementation of a drive based on SPMSM is a brushless direct current (BLDC) motor. In [7], high efficiency, good dynamic characteristics and the potential of BLDC machines for LEV applications are noted, while at the same time paying attention to the problems of electromagnetic torque ripple, electromagnetic interference and noise. For a IWM drive, these characteristics are of particular importance, since electromagnetic ripples are directly transmitted to the wheel.

The optimization problem of SPMSM with concentrated winding for EVs is directly considered in [8]. The work shows that the geometric parameters should be determined not only by the peak torque requirements, but also by electromagnetic, thermal and energy constraints over a wide speed range. This approach creates the basis for the transition from traditional design by the rated point to optimization of the traction machine by the working area.

A useful feature of EVs is the possibility of significantly reducing the installed rated power of the electric motor due to its operation in a fairly wide range of angular velocity regulation with constant power due to the weakening of the magnetic field – Flux Weakening (FW) [9]. In PM electric machines, this is possible due to vector control of the direct i_d and quadrature i_q components of the armature current in the *d-q* reference frame associated with the rotor. In this case, the negative component i_d is used to compensate the PM flux, which allows keeping the back EMF within the available DC bus voltage. The authors in [10] emphasize that the efficiency of FW should be taken into account already at the stage of electromagnetic design of the machine, and not only during the synthesis of the control system. To do this, current and voltage limitations should be taken into account, and an appropriate control strategy should be selected that best provides a compromise between these limitations. For surface-mounted permanent magnet synchronous motor (SPMSM), the problem has an additional feature [8]. Unlike IPMSM, SPMSM is characterized by a small magnetic anisotropy, which leads to the practical equality of inductances along the *d* and *q* axes ($L_d \sim L_q$), so almost all the electromagnetic torque is created by the interaction of the PM flux with the current component i_q. The negative component i_d, required for FW, does not create a useful reluctance torque, but increases the current modulus and, accordingly, copper loss. That is why for SPMSM it is advisable to use a small FW depth so as not to reduce the machine efficiency at high speeds of its operation.

The traditional design of a traction motor based on rated parameters does not fully correspond to the nature of its operation in EVs. Unlike an industrial electric drive with a relatively stable load mode, an EV traction motor operates continuously in a wide range of speeds and torques. Therefore, one of the most informative tools for assessing its energy characteristics is an efficiency map – a display of the dependence of the motor efficiency on the values of angular velocity and torque $\eta(\omega, T)$ [11]. The review [12] systematizes the methods for constructing such maps – analytical, numerical and experimental – and shows the compromise between model accuracy and computational costs. The basis of the efficiency map is the modeling of individual components of energy losses in the motor. Loss in copper is determined by the load current, while loss in iron significantly depend on the frequency and magnitude of the magnetic flux. In addition to these losses, for a PM machine, it is necessary to take into account mechanical losses and additional losses in the rotor and magnets. The relative contribution of these components changes when moving from the high-torque/low-speed region to the high-speed region

[13]. In works [14], [15], [16], different approaches were used to construct efficiency maps for the main types of electric machines: 2D magnetostatic finite elements (FE) modeling for the no-load and short-circuit modes, the results of which are further used together with the *d-q* machine model to construct a loss map in the entire operating region [14]; a limited set of FE modeling or experimental data [15]; analytical and simulation efficiency maps of BLDC traction motor [16]. The results of studies [17] and [18] are particular importance for this work, where the efficiency map is directly related to the parameters of the in-wheel concentrated-winding SPMSM and the characteristic operating points of the drive cycle. Eddy current losses in the PM rotor of machines, which are associated with magnetic field harmonics [19], require separate consideration in SPMSM. An effective means of reducing them is to increase the number of poles and slots in the machine and to segment the PMs.

Using standard drive cycles as the starting point for designing EV drives is the most effective way to ensure high efficiency. Until recently, various drive cycles were used in Japan, the US, and Europe, such as: the JC08, the Urban Dynamometer Driving Schedule (UDDS), the Highway Fuel Economy Driving Schedule (HWFET), and the New European Driving Cycle (NEDC) [20]. Since 2019, a new Worldwide Harmonized Light Vehicles Test Cycle (WLTC) has been introduced to assess the fuel and energy efficiency of light-duty vehicles [21]. Its feature is that new drive cycles of different classes have been created depending on vehicle categories of different power-to-mass ratio (PMR). In particular, Class 1 refers to LEVs with PMR $\leq$ 22 W/kg.

3. RESEARCH AIM AND OBJECTIVES

This work proposes to determine the parameters of an external rotor in-wheel fractional-slot SPMSM for a specific LEV – a new type of electric bicycle (electric fat bike) in such a way as to provide the necessary traction characteristics while simultaneously shifting the area of high motor efficiency to the most energy-significant operating points of the WLTC Class 1 drive cycle. A feature of the developed SPMSM is its operation in two angular velocity regions, both with constant torque and with constant power regulation, which makes it possible to significantly reduce the rated motor power compared to the base model. To achieve the goal set in the work, it is necessary to determine the range of the most frequent values of the angular velocity and torque of the motor to ensure the selected LEV operation in a given drive cycle. Based on the results obtained, the main parameters of the motor should be substantiated, which will ensure its effective operation in the two speed region. To verify the obtained results, it is necessary to create an efficiency map of the developed motor and use it to conduct a computer simulation of the operation of the LEV under study in the WLTC Class 1 cycle. The effectiveness of the proposed approach is verified by comparing the operation of the LEV under study with the developed and baseline electric drive systems.

4. MATERIALS AND METHODS

4.1 Determination of rated and maximum output parameters of the SPMSM for the LEV under study

4.1.1 Experimental LEV and its parameters

The SAMEBIKE M20-III 2000W 36Ah [22] electric fat bike with large drivivng range was chosen as the LEV under study (Fig. 1). This e-bike features wider tires than traditional models, which improves its all-terrain performance, and a higher-capacity battery to handle challenging terrain and steep inclines. Its main parameters are listed in Table 1.



Fig. 1. **LEV under study**
***Source*: obtained by the authors from [21]**

Table 1. **Main parameters of the LEV under study**

Parameter	Value
Li-ion battery capacity	36 A·h
Rated battery voltage	48 V
Rated motor power	2000 W
Maximum speed	up to 60 km/h
Transmission	Shimano Tourney 7-speed
Assist mode range	up to 280 km
Electric-only range	up to 140 km
Wheel diameter	20 in
LEV mass	38 kg
Maximum payload capacity	up to 180 kg

***Source*: obtained by the authors from [22]**

ISSN 2663-0176 (Print)
ISSN 2663-7731 (Online)

4.1.2 Determination of the required torque and angular velocity values of the traction motor for the LEV executing the WLTC Class 1 cycle

The key initial parameters for further research are the ranges of angular velocity and torque of the traction motor (where it works most of the time in the driving cycle), which can be determined by having the corresponding histograms of its operation in traction mode. To obtain a data set and build histograms, the experimental driving cycle for light vehicles WLTC class 1 (Fig. 2) was chosen as the starting point, which was downloaded in digitized form from [23] as an Excel file.

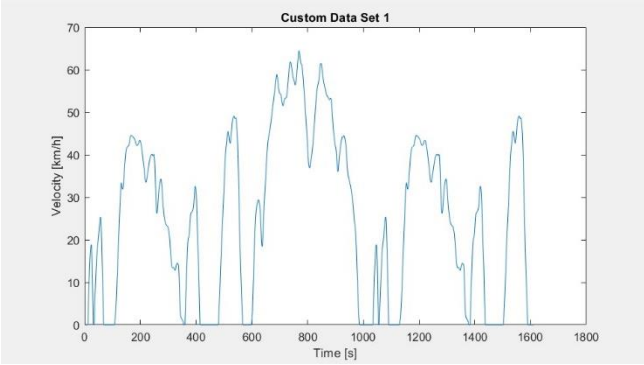


Fig. 2. **WLTC class 1 drive cycle**

***Source*: obtained by the authors from [23]**

The set of experimental data required for constructing the histogram (of angular velocity ω and torque T) was obtained using a computer model built in the MATLAB/Simulink environment (Fig. 3), which used the aforementioned drive cycle.

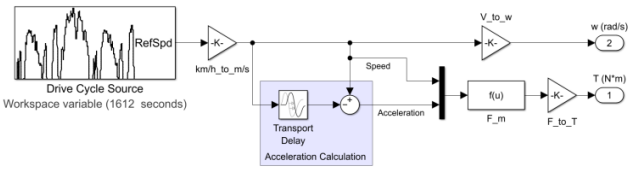


Fig. 3. **Computer model for calculating angular velocity and electromagnetic torque during the movement of the LEV under study in the WLTC Class 1 drive cycle**

***Source*: compiled by the authors**

The Drive Cycle Source subsystem generates a test drive cycle, which is given by the corresponding MATLAB workspace variable obtained as a result of the work of the script implemented by the authors, which allowed reading data from the aforementioned Excel file. The highlighted Acceleration Calculation zone implements the calculation of the LEV acceleration by subtracting from the current value of the movement speed the previous one, obtained using the Transport Delay block with a delay setting of 1 s. The F_m function block implements the calculation of the total traction force of the LEV linear movement:

$$F_{\text{t}} = F_{\text{roll}} + F_{\text{drag}} + m\,a\,, \tag{1}$$

where F_{roll} is the rolling resistance force, F_{drag} is the aerodynamic drag force, m is the LEV mass with driver, and a is the LEV acceleration.

The forces included in (1) are described by the following well-known expressions:

$$F_{\text{roll}} = \begin{cases} f_{\text{d}}\, m\, g\, \cos\gamma, & V > 0 \\ 0, & V = 0 \end{cases}, \tag{2}$$

$$F_{\text{drag}} = 0.5\,\rho_{\text{a}}\, A_{\text{f}}\, c_{\text{d}}\, V^2\,, \tag{3}$$

where f_{d} is the rolling resistance coefficient, γ is the road slope angle, assumed to be zero in this case, ρ_{a} is the air density, A_{f} is the frontal area of the LEV with a driver, c_{d} is the aerodynamic drag coefficient, and V is the LEV speed.

The values of the parameters included in equations (1)-(3) are given in Table 2.

Table 2. **Parameters of equation (1)-(3)**

Parameter	Value
m	218 kg
f_{d}	0.015
ρ_{a}	1.23 kg/m^3
A_{f}	0.5 m^2
c_{d}	0.22

***Source*: compiled by the authors**

To convert the linear velocity of the LEV into the angular velocity of the wheel, and therefore the motor rotor, and to convert the traction force into motor torque, the V_to_w and F_to_T blocks are used with gain coefficients $1/r_{\text{w}}$ and r_{w}, respectively, where r_{w} is the wheel radius.

4.1.3 . Dynamics of required angular velocity and torque values for the traction motor and derivation of requirements for SPMSM output parameters

The time diagrams of the angular velocity and torque of the drive motor of the LEV under study obtained using the computer model shown in Fig. 3 during the execution of the WLTC Class 1 drive cycle are shown in Fig. 4. As can be seen from the obtained results, in the process of working out the drive cycle, the maximum value of the motor angular velocity reaches ω_{max} = 65.6 rad/s, and the

maximum value of the traction torque is T_{max} = 54.8 N·m.

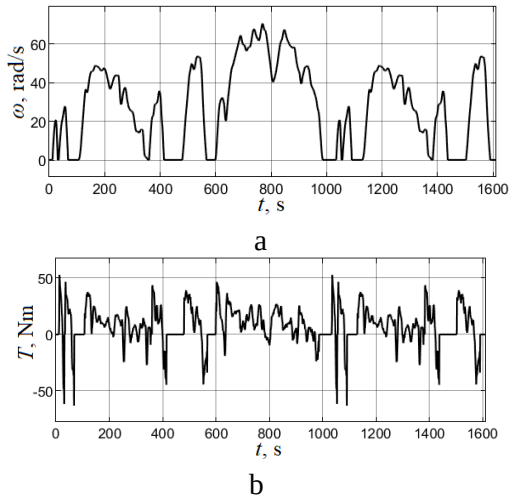


Fig. 4. **Time diagrams of main variables obtained during the execution of the WLTC Class 1 drive cycle by the LEV under study: a –angular velocity; b – motor torque**

***Source*: compiled by the authors**

In order to assess the frequency of repetition of combinations of angular velocity and torque values, the results shown in Fig. 4 are presented in the form of a histogram, which is shown in Fig. 5. The histogram used a division of the entire range of angular velocity and motor torque into 10x10 corresponding units. Data filtering by operating mode was performed programmatically using a MATLAB script implemented by the authors. As can be seen from Fig. 5, most of the time in traction mode the LEV drive operates in the range of rotation speed (0 – 630) rpm or (0 – 66.0) rad/s and torque (0 – 39) Nm, and the apparent maxima of these coordinates are in the ranges Δn_{max} = (350 – 500) rpm or $\Delta\omega_{max}$ = (36.7 – 52.4) rad/s and ΔT_{max} = (0 – 39) Nm. The latter range is advisable to design the zone of maximum motor efficiency values for the drive of the LEV under study.

4.2 Calculation of required motor parameters

The zones of maximum values of angular velocity and motor torque obtained in section 4.1.3, required for the LEV work out the WLTC Class 1 drive cycle, in relative units with respect to the corresponding maximum values of ω_{max} and T_{max}, are $\Delta\omega^*_{max}$ = (0.56 – 0.80) and ΔT^*_{max} = (0 – 0.60). The analysis of typical efficiency maps for different types of electric machines conducted in [24] shows that the maximum of the efficiency map for SPMSM is approximately in the same range, provided that the angular velocity adjustment range in the FW region is approximately equal to $D_{FW} = \omega_{max} / \omega_n = 2$. Therefore, for the LEV drive, we will design an SPMSM specifically to ensure such a range. The effectiveness of the decision will be verified by comparing the efficiency of the LEV under study in the WLTC Class 1 drive cycle with two SPMSM variants. The first one is the experimental SPMSM with FW control in the speed range D_{FW} = 2 and the second one is a typical SPMSM, which operates only in the constant torque region, and therefore its rated angular velocity is equal to the maximum required value $\omega_n = \omega_{max}$.

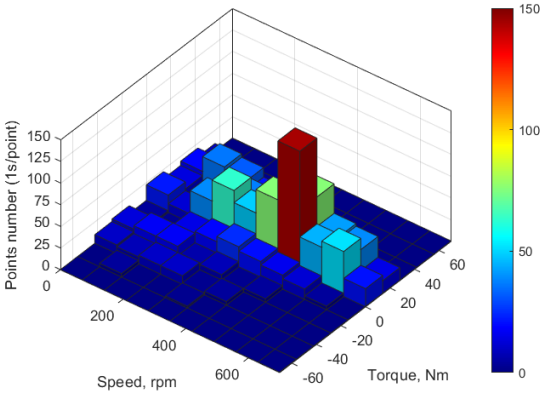


Fig. 5. **Histogram of rotational speed and torque during the execution of the WLTC Class 1 drive cycle by the LEV under study**

***Source*: compiled by the authors**

4.2.1 Features of a SPMSM operation in the FW region

During of a SPMSM operation, a back-EMF is generated in motor windings and directed opposite to the supply voltage with an amplitude of

$$E_m = p_p \psi_d \omega, \quad (4)$$

where p_p is the number of pole pairs of the motor and ψ_d is the resultant flux linkage of the SPMSM (aligned along the *d*-axis in the vector diagram).

When the motor reaches its rated angular velocity (if we neglect the voltage drop across the winding resistance), the back-EMF becomes practically equal to the supply voltage, which makes it impossible to implement angular velocity regulation above its rated value.

The equation of the *d*-component of the SPMSM flux linkage is described by the equation

$$\psi_d = \psi_{pm} + L_d i_d, \quad (5)$$

where ψ_{pm} is the PM flux linkage (aligned along the *d*-axis).

ISSN 2663-0176 (Print)
ISSN 2663-7731 (Online)

According to (5), the introduction of a negative value of i_d allows creating a counter magnetic flux, which will weaken the effect of the PM flux – providing FW. This will lead to a decrease in the EMF according to (4) and will allow regulating the angular velocity of the motor above its rated value.

However, such control is subject to two constraints: current and voltage limits [9]:

– the current limit is associated with ensuring the permissible heating of the armature winding for a given value of the torque-producing current component i_q

$$i_{\max}^2 \geq i_d^2 + i_q^2, \quad (6)$$

where $i_{\max}$ is the maximum amplitude of the motor armature current, limited by its cooling conditions;

– the voltage limit is caused by a specific value of the inverter DC supply voltage (battery voltage) v_{DC} and the selected PWM strategy

$$v_{\max}^2 \geq v_d^2 + v_q^2, \quad (7)$$

where $v_{\max}$ is the maximum amplitude of the motor armature voltage, which, when using space vector PWM, is related to v_{DC} by the expression

$$v_{\max} = v_{DC} / \sqrt{3}. \quad (8)$$

The mathematical model of the PMSM in the *d-q* reference frame is expressed as follows [7]:

$$v_d = R i_d + L_d \frac{\mathrm{d}}{\mathrm{d}t} i_d - p_p \omega L_q i_q, \quad (9)$$

$$v_q = R i_q + L_q \frac{\mathrm{d}}{\mathrm{d}t} i_q + p_p \omega L_d i_d + p_p \omega \psi_{pm}, \quad (10)$$

$$T = \frac{3}{2} p_p \left[\psi_{pm} i_q + \left(L_d - L_q \right) i_d i_q \right], \quad (11)$$

where R is the armature winding resistance.

Substituting equations (9) and (10) into (7) and neglecting the armature winding resistance, the voltage limit for the PMSM steady-state operation takes the form

$$\left(p_p \omega L_q i_q \right)^2 + \left(p_p \omega L_d i_d + p_p \omega \psi_{pm} \right)^2 \leq v_{\max}^2. \quad (12)$$

In the current component referece frame (i_d - i_q), constraint (12) represents the equation of an ellipse centered at ($-\psi_{pm}/L_d$, 0). However, in the case of an SPMSM, where $L_d = L_q = L$, this constraint transubstantiates into a circle. Thus, it is convenient to represent the current and voltage limits for the vector control of the SPMSM in the form of the circle diagrams shown in Fig. 6.

When the SPMSM operates at speeds below the rated value $\omega < \omega_n$, the optimal strategy for minimizing the copper loss in the machine is $i_d = 0$, which is called maximum torque per ampere (MTPA) [9]. For a given torque value T, this will be reflected by the operating point "A", which is located inside the limitation circles current $i_{\max}$ (red circle) and voltage $v_{\max}$ (blue dashed circle). To increase the angular velocity $\omega > \omega_n$ for a given limit $v_{\max}$, the radius of the voltage limitation circle will decrease, so to stay in this circle, it is necessary to introduce a current component $i_d < 0$. For the previous value of the motor torque, this will mean moving from the operating point "A" to the left until reaching point "B", which is located on the red circle. Therefore, for a further increase in the angular velocity, it is necessary to follow the current limitation – the transition from point "B" to point "C". An even greater increase in the angular velocity is possible with the maximum torque per volt (MTPV) strategy – the transition from point "C" to point "D" (critical). As can be seen from the diagrams in Fig. 6, an increase in angular velocity in the FW zone is inevitably associated with a decrease in the maximum value of the electromagnetic torque.

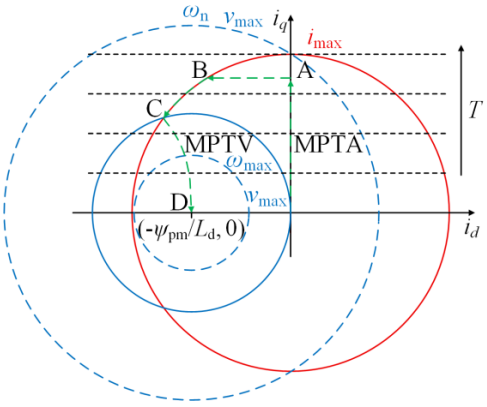


Fig. 6. **Constraint diagram for vector control of SPMSM operation over a wide speed range**

***Source*: compiled by the authors based on [9] and [10]**

4.2.2 Determination of the main parameters of SPMSM taking into account current and voltage limitations

Equations (4) and (12) allow us to select the main parameters of SPMSM. The number of pole pairs depends on the rated parameters and design of the SPMSM. With a decrease in the rated angular velocity of the PM motor, the number of its poles increases [7]. It is also somewhat larger for machines with an external rotor. In addition, as studies [8] show, with an increase in the number of rotor pole pairs and stator slots of the SPMSM, the

losses in the permanent magnets, which can be significant in this machine, rapidly decrease. Based on all these considerations, $p_p = 10$ is adopted in the experimental SPMSM for the LEV under study.

The value of E_m obtained by (4) at the rated angular velocity ω_n is the limited value of the voltage in the DC bus v_{DC}. Without taking into account the voltage drop across the armature winding resistance and taking into account the known dependence for the maximum achievable amplitude of the phase sinusoidal voltage at the output of the three-phase inverter (8), equating v_{max} and E_m, we obtain the following inequality to justify the required value of flux linkage due to PM:

$$\psi_{pm} \le \frac{v_{DC}}{\sqrt{3}\, p_p\, \omega_n}. \quad (13)$$

From (11) we can find the value of the maximum SPMSM armature current required to provide the maximum electromagnetic torque $T_{max} = k_T T_n$,, where k_T is the overload capacity ratio of the motor:

$$i_{max} = \frac{2 k_T T_n}{3 p_p \psi_{pm}}. \quad (14)$$

Expression (14) was obtained taking into account that in the MTPA mode, to ensure maximum SPMSM efficiency, the armature current component i_d must be equal to zero, since only the component i_q is torque-generating.

Expressions (4) and (14) correspond to the SPMSM operation in the region from zero to the rated value of angular velocity – constant torque control. For a further increase in the angular velocity up to its maximum value ω_{max}, the machine must operate in the control zone with constant power. To satisfy equation (4) and inequality (13) at a constant value of v_{DC} and an increase in ω, the resulting flux linkage must decrease, as was shown in subsection 4.2.1. This is achieved by means of FW – vector control of the armature current components: by introducing a negative value of the component i_d, which will weaken the flux from the PM, and by providing the value of the component i_q required to generate the specified electromagnetic torque.

The main parameter of the PMSM, which directly affects the angular velocity regulation range in the FW region, is the armature winding inductance L_d [8].

To expand the speed regulation region, this value of L_d must satisfy the inequality:

$$L_d \ge \frac{\psi_{pm}}{i_n}, \quad (15)$$

where i_n is the rated motor armature current.

As mentioned in Section 1, for SPMSM, in order to ensure high efficiency, it is not advisable to plan a wide range of speeds in the FW operating zone. Therefore, we will take the acceptable value of this range for study drive $D_{FW} = 2$ and determine the value of L for SPMSM, which provide such a range based on the fulfillment of the necessary of current and voltage constraints shown in Fig. 6.

The modulus of any current vector must be less than i_{max}, which is determined by (6). At the end of the speed range, the value of the maximum motor torque will be D_{FW} times smaller, respectively, the torque-generating component of the armature current will be equal to

$$i_{q.FW} = \frac{2 k_T T_n}{3 p_p \psi_{pm} D_{FW}}. \quad (16)$$

To fulfill the current limitation condition, the i_d component of the armature current must not exceed the value

$$i_{d.FW} = \sqrt{i_{max}^2 - i_{q.FW}^2}. \quad (17)$$

The minimum armature winding inductance value L_{min} is determined from the flux linkage constraint inequality for the maximum motor angular velocity at the end of the FW range:

$$L_{min}^2 \left(I_{max}^2 - i_{d.FW}^2\right) + \left(\psi_{pm} + L_{min} i_{d.FW}\right)^2 \le \left(\frac{v_{max}}{p_p\, \omega_{max}}\right)^2. \quad (18)$$

From inequality (18), the following minimum value of the armature winding inductance is obtained:

$$L_{min} = \frac{-\psi_{pm} i_{d.FW} - \sqrt{\left(\psi_{pm} i_{d.FW}\right)^2 - i_{max}^2 \left[\psi_{pm}^2 - v_{max}^2 / \left(p_p \omega_{max}\right)^2\right]}}{i_{max}^2}. \quad (19)$$

The maximum value of the armature winding inductance L_{max} is determined from the voltage limitation condition for the initial rated angular velocity of the motor for the FW range:

$$\left(p_p \omega_n i_{max} L_{max}\right)^2 + \left(p_p \omega_n \psi_{pm} + i_{max} R\right)^2 \le v_{max}^2 \quad (20)$$

From inequality (20) the following maximum value of the armature winding inductance is obtained:

ISSN 2663-0176 (Print)
ISSN 2663-7731 (Online)

$$L_{\max} = \frac{\sqrt{v_{\max}^2 - \left(p_{\mathrm{p}}\omega_{\mathrm{n}}\psi_{\mathrm{pm}} + i_{\max}R\right)^2}}{p_{\mathrm{p}}\omega_{\mathrm{n}}i_{\max}}. \quad (21)$$

Equations (19) and (21) determine the range of inductance of the SPMSM armature winding, which simultaneously provides the maximum electromagnetic torque of the motor and the possibility of operation in the FW zone with the angular velocity control range D_{FW}.

Taking into account the adopted value of $D_{\mathrm{FW}} = 2$ and the required maximum values of the angular velocity and torque of the motor, we obtain their rated values for the experimental SPMSM, which are given in the second column of Table 3. The other parameters of the experimental SPMSM for the LEV under study, justified above and calculated using expressions (13)-(21), are also shown there.

The third column of Table 3 shows the corresponding basic parameters for the typical SPMSM, which should operate only in the constant torque region. Since its rated angular velocity is twice as high as the rated angular velocity of the experimental SPMSM, the rated power also doubles. The increase in the rated angular velocity of the typical SPMSM leads to a reasonable reduction in the number of its pole pairs, which is taken to be $p_{\mathrm{p}} = 6$. According to expressions (13)-(15), other parameters of the typical SPMSM are also found.

Table 3. **Parameters of SPMSMs for the LEV under study**

Parameters	Values	
	Experimental	Typical
Rated power, P_{n} (W)	900	1800
Rated angular velocity, ω_{n} (s^{-1})	32.8	65.6
Rated torque, T_{n} (Nm)	27.4	27.4
Number of pole pairs, p_{p}	10	6
PM flux linkage, ψ_{pm} (Wb)	0.048	0.040
Winding inductance, L (mH)	0.80	0.60

***Source*: compiled by the authors**

The efficiency of the SPMSM is equal to the ratio of the mechanical power at the machine output P_{out} to the active electrical power at its input P_{in}:

$$\eta = \frac{P_{\mathrm{out}}}{P_{\mathrm{in}}}. \quad (22)$$

The mechanical output power is equal to the product of the electromagnetic torque and the angular velocity of the machine:

$$P_{\mathrm{out}} = T\,\omega. \quad (23)$$

The active electric power at the input of the machine is equal to the dot product of the armature voltage and armature current vectors, which can be represented by the following expression:

$$P_{\mathrm{in}} = \left(\vec{v}\cdot\vec{i}\right) = \left|\vec{v}\right|\left|\vec{i}\right|\cos\varphi = \frac{3}{2}\sqrt{v_d^2+v_q^2}\,\sqrt{i_d^2+i_q^2}\,\cos\left(\operatorname{atan}\frac{v_d}{v_q} - \operatorname{atan}\frac{i_d}{i_q}\right) \quad (24)$$

where φ is the the angle between the armature voltage and current vectors.

4.3 Modeling the main losses in the machine and building its efficiency map

4.3.1 Mathematical description of SPMSM dynamics taking into account losses in copper and iron

Let us assume in the first approximation that the magnetic circuit is not saturated and that the inductance of the motor armature winding is independent of the rotor position. Under these conditions, the equivalent circuit of the SPMSM, taking into account the iron losses, will take the form shown in Fig. 7, where R_{c} is the resistance that models the iron losses [25].

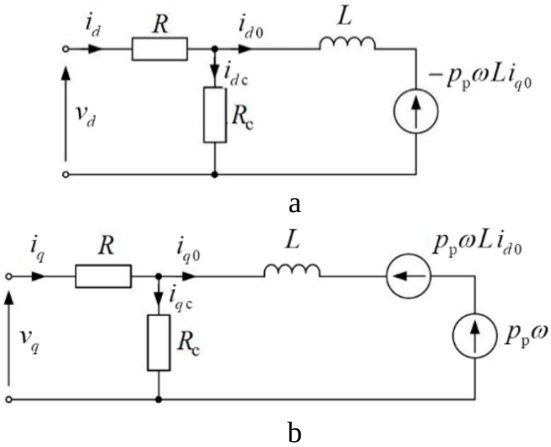


Fig. 7. **Equivalent circuits of SPMSM considering coper and iron losses: a – relative to the *d* axis; b – relative to the *q* axis**

***Source*: compiled by the authors**

Based on the equivalent circuit shown in Fig. 7, the electrical equilibrium equation of the SPMSM in a rotating *d-q* reference frame oriented by the PM field of the rotor can be described by the following systems of equations [26]:

$$\begin{cases} i_d = i_{d0} + \dfrac{1}{R_c}\left(L\dfrac{\mathrm{d}}{\mathrm{d}t} i_{d0} - p_p \omega L i_{q0} \right) \\ i_q = i_{q0} + \dfrac{1}{R_c}\left(L\dfrac{\mathrm{d}}{\mathrm{d}t} i_{q0} + p_p \omega L i_{d0} + p_p \omega \psi_{pm} \right) \end{cases}, \quad (25)$$

$$\begin{cases} v_d = i_d R + L\dfrac{\mathrm{d}}{\mathrm{d}t} i_{d0} - p_p \omega L i_{q0} \\ v_q = i_q R + L\dfrac{\mathrm{d}}{\mathrm{d}t} i_{q0} + p_p \omega L i_{d0} + p_p \omega \psi_{pm} \end{cases}. \quad (26)$$

Substituting (25) into (26), we obtain:

$$\begin{cases} L\dfrac{\mathrm{d}}{\mathrm{d}t} i_{d0} = -L i_{d0} \dfrac{R}{L_d A} + p_p \omega L_q i_{q0} + \dfrac{1}{A} v_d \\ L\dfrac{\mathrm{d}}{\mathrm{d}t} i_{q0} = -L i_{q0} \dfrac{R}{L_q A} - p_p \omega \left(L_d i_{d0} + \psi_{pm} \right) + \dfrac{1}{A} v_q \end{cases}, \quad (27)$$

where

$$A = 1 + \frac{R}{R_c}. \quad (28)$$

In addition to the system of equations (27), the SPMSM mathematical model also includes the differential equation for the motor shaft torque balance:

$$J_m \frac{\mathrm{d}}{\mathrm{d}t} \omega = T - T_L, \quad (29)$$

where J_m is the moment of inertia of the drive, reduced to the motor shaft, and T_L is the static load torque on the motor shaft.

The electromagnetic torque of the investigated SPMSM is described by equation

$$T = \frac{3}{2} p_p \psi_{pm} i_{q0}. \quad (30)$$

Thus, the complete mathematical model of SPMSM taking into account coper and iron losses has the following form:

$$\begin{cases} L\dfrac{\mathrm{d}}{\mathrm{d}t} i_{d0} = -i_{d0} \dfrac{R}{A} + p_p \omega L_d i_{q0} + \dfrac{1}{A} v_d \\ L\dfrac{\mathrm{d}}{\mathrm{d}t} i_{q0} = -i_{q0} \dfrac{R}{A} - p_p \omega \left(L_d i_{d0} + \psi_{pm} \right) + \dfrac{1}{A} v_q \\ J_m \dfrac{\mathrm{d}}{\mathrm{d}t} \omega = \dfrac{3}{2} p_p \psi_{pm} i_{q0} - T_L \end{cases}. \quad (31)$$

4.3.2 Parameter determination of the investigated SPMSM modeling copper and iron losses

Let us find, with a reasonable approximation, expressions for determining the main parameters of the SPMSM that model losses in copper and iron, respectively, the values of the resistances R and R_c, based on its given rated energy loss indicators – relative copper loss δ_{Cu} and relative iron loss δ_{Fe}.

To determine the value of the resistance of the SPMSM armature winding, we neglect the losses in iron and assume $R_c = \infty$. Then, based on the SPMSM equivalent circuit shown in Fig. 7, controlled according to the MTPA strategy ($i_{d0} = 0$), the relative energy loss in the copper of the machine winding in the rated mode will be equal to

$$\delta_{Cu} = \frac{\Delta P_{Cu}}{P_n + \Delta P_{Cu}} = \frac{3/2 \cdot i_{q0.n}^2 R}{3/2 \cdot p_p \psi_{pm} i_{q0.n} \omega_n + 3/2 \cdot i_{q0.n}^2 R} = \left(\frac{p_p \omega_n \psi_{pm}}{i_{q0.n} R} + 1 \right)^{-1}, \quad (32)$$

where ΔP_{Cu} is the absolute copper power loss, and $i_{q0.n}$ is the rated value of the armature current projection onto the q axis.

From (32), we obtain:

$$R = \frac{p_p \omega_n \psi_{pm}}{i_{q0.n} \left(\delta_{Cu}^{-1} - 1 \right)}. \quad (33)$$

Assuming δ_{Cu} = 3.5 %, according to (33), in accordance with the rated parameters given in Table 3, for the experimental SPMSM R = 0.015 Ohm was obtained, and for the typical SPMSM R = 0.0086 Ohm was obtained.

From the equivalent circuit shown in Fig. 7, the relative power loss in the SPMSM iron can be represented by the power loss in the resistance R_c, which models them. For the rated operating mode, we can write [26]

$$\delta_{Fe} = \frac{\left(p_p \omega_n \psi_{pm} \right)^2}{R_{c.n} P_n}, \quad (34)$$

where $R_{c.n}$ is the value of the resistance R_c in the rated operating mode of the SPMSM.

Assuming δ_{Fe} =4.0 %, according to (34), in accordance with the rated parameters given in Table 3, for the experimental SPMSM $R_{c.n}$ = 6.89 Ohm was obtained, and for the typical SPMSM $R_{c.n}$ = 3.44 Ohm was obtained.

The power losses due to hysteresis and eddy currents, which together constitute the iron loss, vary depending on the angular velocity of the machine. As a result, this leads to a decrease in the resistance value R_c with decreasing angular velocity. As shown in [27], this trend can be modeled quite accurately by the following equation:

ISSN 2663-0176 (Print)
ISSN 2663-7731 (Online)

$$R_{\mathrm{c}} = R_{\mathrm{c.n}} \frac{\frac{K_{\mathrm{f}}}{K_{\mathrm{h}}} + 1}{\frac{K_{\mathrm{f}}}{K_{\mathrm{h}}} + \frac{1}{\omega^*}}, \quad (35)$$

where K_{h} and K_{f} are the relative values of power losses due to hysteresis and eddy currents for the rated SPMSM mode (according to experimental data obtained in [27], $K_{\mathrm{f}} / K_{\mathrm{h}} = 0.5694$), and ω^* is the relative angular velocity $\omega^* = \omega/\omega_{\mathrm{n}}$.

For steady-state operation of the SPMSM taking into account coper and iron losses, the system of equations (31) is transformed to the following form:

$$\begin{cases} v_d = R i_{d0} - A\, p_{\mathrm{p}}\, \omega L i_{q0} \\ v_q = R i_{q0} + A\, p_{\mathrm{p}}\, \omega \left(L i_{d0} + \psi_{\mathrm{pm}} \right). \\ T_{\mathrm{L}} = \frac{3}{2} p_{\mathrm{p}}\, \psi_{\mathrm{pm}}\, i_{q0} \end{cases} \quad (36)$$

The useful for mathematical modeling dependencies between currents in the steady-state mode of SPMSM operation, taking into account coper and iron losses, can be obtained from the original systems of equations (25) and (26). Expressing $L_d \frac{\mathrm{d}}{\mathrm{d}t} i_{d0}$ from the first equation of system (25) and substituting it into the first equation of system (26), as well as expressing $L_q \frac{\mathrm{d}}{\mathrm{d}t} i_{q0}$ from the second equation of system (25) and substituting it into the second equation of system (26), after transformations we obtain

$$\begin{cases} i_d = \frac{1}{A} i_{d0} + \frac{1}{R_{\mathrm{c}} A} v_d \\ i_q = \frac{1}{A} i_{q0} + \frac{1}{R_{\mathrm{c}} A} v_q \end{cases}. \quad (37)$$

4.3.3 Study of the operational efficiency of the experimental and typical SPMSMs on the variable plane "angular velocity – torque" and design of their efficiency maps

The study of the operational efficiency of the SPMSM was carried out according to its mathematical model, represented by the systems of equations (31) and (37). Based on these, a computer model of the electric drive system with vector control of the components of the motor currents i_{d0} and i_{q0} was built in the MATLAB/Simulink environment (Fig. 8). Since in this study we are interested in the value of the electric machine efficiency for various combinations of its angular velocity and electromagnetic torque only in the steady-state mode of its operation, a number of simplifications were introduced into the model. The first one is the assumption of the sinusoidal nature of the basic variables; therefore, the machine was modeled in *d-q* reference frame. The second one is that control is carried out by adjusting the modules of the *d-q* components of the armature voltage without taking into account the operation of the power converter and PWM. The third one is that saturation of the magnetic core and mutual inductance between the phases windings of the armature were not taken into account. And the last one is that the moment of inertia of the drive is taken small in order to speed up the simulation.

The reference angular velocity w_ref is fed to the speed controller SR (a PI controller with lsaturation), the output of which forms the electromagnetic torque reference T^* for the "Electromagnetic Part" subsystem, which reproduces the system of equations for the SPMSM accounting for iron loss (31). The input of this subsystem also includes the reference of the longitudinal component of the armature current $id0^*$ and the value of the angular velocity from the output of the machine mechanical part. The latter, with a moment of inertia $J = 3$ kg·m^2 and a given static load torque T_load, receives the value of the electromagnetic torque T calculated in the "Electromagnetic Part" subsystem.

The "Electromagnetic Part" subsystem (Fig. 9) forms two closed loops for regulating the armature current components with the corresponding current controllers CRd and CRq: the set values i_{d0} and i_{q0} calculated to obtain the required value of the electromagnetic torque. At the output of the specified controllers, after compensation of cross-couplings, the required values of the armature input voltage components v_d and v_q are formed. The function block Fcn2 calculates the exact value of the resistance R_{c}, which models the iron loss using (35), and the function block Fcn3 calculates the corresponding value of the coefficient A using (28) based on the obtained value R_{c}. The latter is used in the model itself both for calculating the values of the armature current components i_{d0} and i_{q0} by integrating equations (27), and for calculating the components i_d and i_q of the SPMSM input current based on equations (37) using the Fcn1 blocks.

The obtained values of the components of the input armature voltage v_d and v_q are used in the

"V_DC Subsystem" (Fig. 8) to determine the required value of the DC voltage of the inverter supply. These same components of the SPMSM armature input voltage together with the components of the input armature current i_d and i_q are fed to the input of the "Input Power Subsystem", where the required value of the motor input power for the conditions under study is calculated using (24). The latter, together with the output mechanical power of the machine, allows us to obtain the desired value of the SPMSM efficiency.

Through the coordinate transformation blocks dq0→abc (Fig. 8), the current values of the phase voltage Vs and the phase current Is of the machine stator are calculated, which makes it possible to estimate the displacement angle between them.

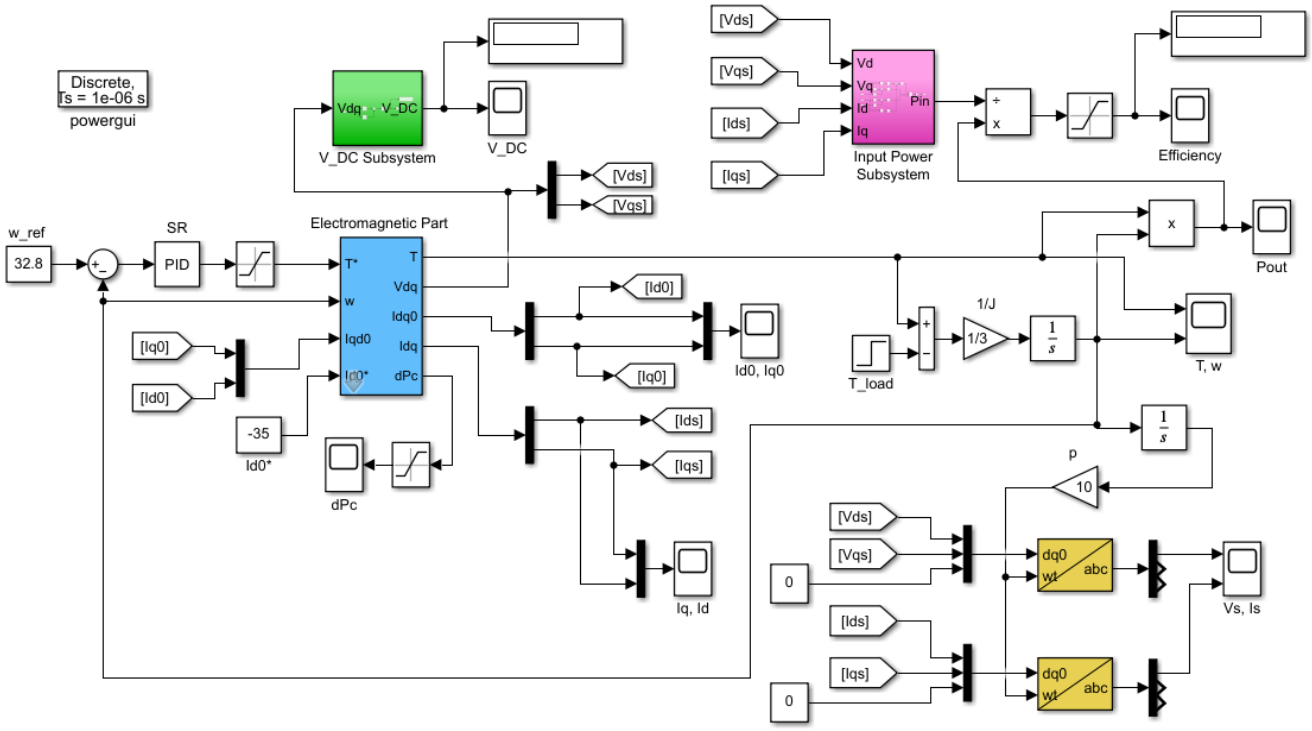


Fig. 8. **Computer model for studying the operational efficiency of the SPMSM**

***Source*: compiled by the authors**

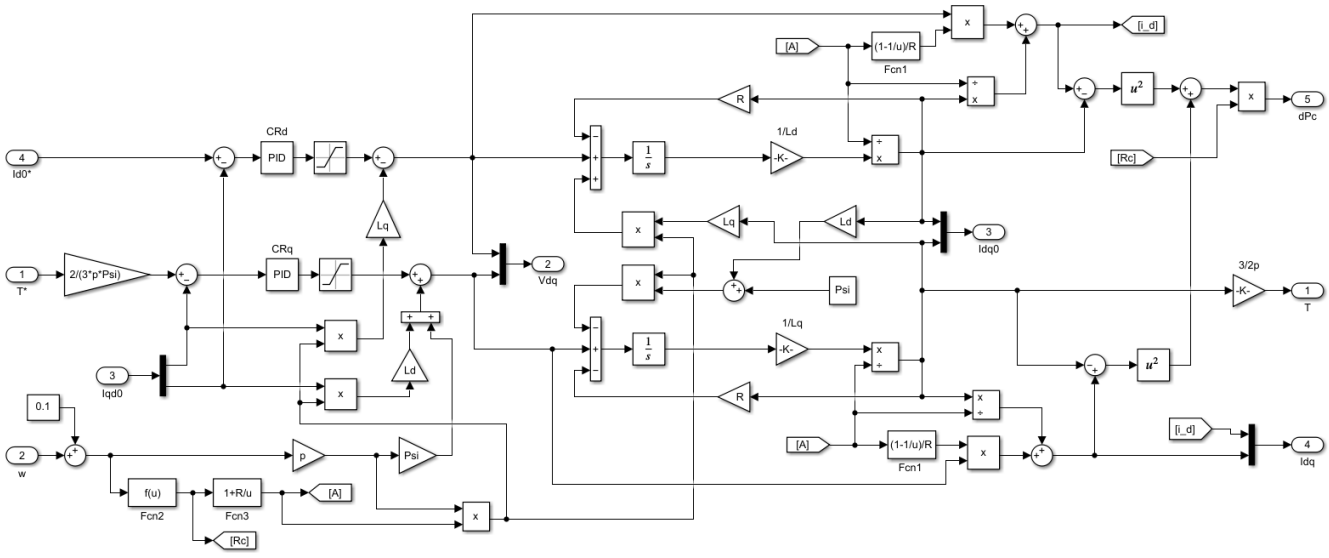


Fig. 9. **Computer model of the Electromagnetic Part subsystem of the SPMSM**

***Source*: compiled by the authors**

ISSN 2663-0176 (Print)
ISSN 2663-7731 (Online)

Using the developed computer model, two cycles of research on the operation efficiency were carried out, respectively, for the experimental and typical SPMSMs in the entire range of changes in their angular velocity ω and load torque T_{load}.

At the point of steady-state operation, the electromagnetic torque of the machine is equal to the static load torque $T = T_{load}$. The points for the study were changed with a gradation of 0.2 from the rated value. For each pair of given variables, the maximum efficiency value was searched for by changing the reference i_{d0}. For the experimental SPMSM in the FW region, the torque value was increased until the desired v_{DC} value exceeded the rated value of 48 V.

The results of the studies for the experimental SPMSM are presented in Fig. 10.

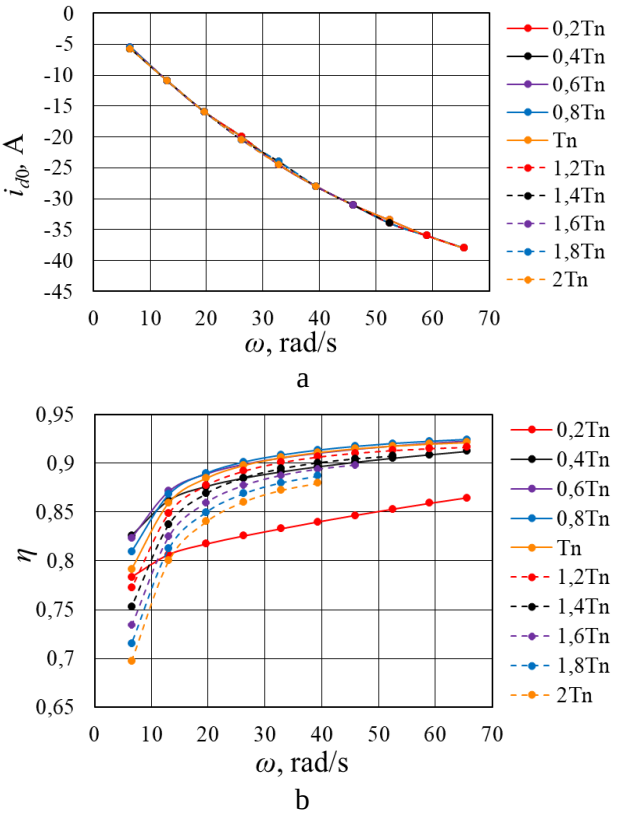


Fig. 10. **Obtained dependences on the angular velocity and torque for the experimental SPMSM:**
a - optimal value of the armature current component i_{d0}; b - maximum efficiency
***Source*: compiled by the authors**

As studies have shown, the maximum efficiency for each value of the motor angular velocity were achieved at the same optimal value of the armature current component i_{d0}. These values for the experimental SPMSM are shown in Fig. 10a, from which it is clear that the modulus of the i_{d0} value increases with increasing angular velocity of the machine. At the same time, in the constant torque region, the growth rate of the modulus of the i_{d0} value is greater than one in the constant power region. For a typical SPMSM, the optimal dependence $i_{d0}(\omega)$ has a similar character, but the current values are smaller in magnitude.

Fig.10b, shows a family of maximum efficiency curves versus angular velocity and torque of the experimental SPMSM, which is not visually revealing as the efficiency maps.

To construct the efficiency maps of SPMSMs, the computer program Surfer was used. The efficiency maps obtained from the results of the computer experiments in the form of isolines of constant efficiency for two SPMSMs, the experimental and the typical, are shown in Fig. 11. As can be seen from them, both SPMSMs provide zones of maximum efficiency in the ranges required for the LEV under study operating in the WLTC class 1 drive cycle. However, the zone of maximum torque limitation in the experimental SPMSM is significantly larger than in the typical SPMSM, which is due to FW.

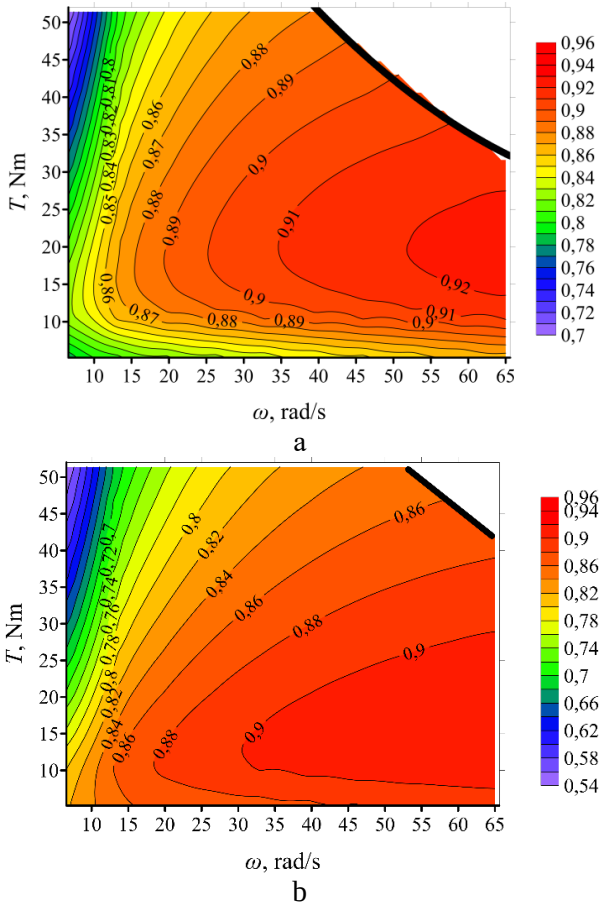


Fig. 11. **Obtained efficiency maps:**
a – for experimental SPMSM;
b – for typical SPMSM
***Source*: compiled by the authors**

5.RESEARCH RESULTS

5.1 Computer simulation of the LEV under study operation using the EMR method

In order to investigate the performance efficiency of the LEV during the WLTC class 1 drive cycle, a computer model was built using the Energetic Macroscopic Representation (EMR) method [28], [29]. The advantage of this method is a macroscopic view of the system from the point of view of the energy processes taking place in it. It allows to highlight the general energy patterns of interaction between the main subsystems based on simple dependencies without secondary features, which ensures the high speed of simulation and the possibility of modeling long real-time segments, such as drive cycles. In addition, the EMR provides a unified construction of a process control system based on the inversion principle.

The developed EMR model of the LEV under study with in-wheel SPMSM is shown in Fig. 12.

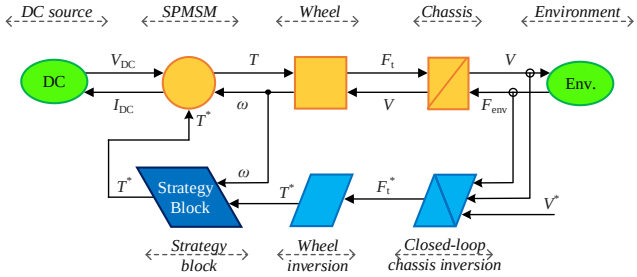


Fig. 12. **EMR model of the LEV under study with in-wheel SPMSM**

***Source*: compiled by the authors**

The "DC source" subsystem, for example, a battery, is modeled by an EMF source E_B with an internal resistance R_B:

$$V_{DC} = E_B - I_{DC} R_B . \quad (38)$$

The "SPMSM" subsystem models the operation of the traction motor in the simplest possible way, providing inertia-free and astatic regulation of the given value of the electromagnetic torque T^* – in fact, this is the transfer of T^* from input 3 to output 1 (Fig. 13). The main task of this subsystem is to ensure the transfer of power from input to output in the traction mode, when a positive torque is set, and vice versa in the regenerative braking mode, when the given torque is negative. This is done with the Switch key. In addition, the subsystem takes into account copper and iron losses of the motor using the obtained efficiency map recorded in the Look-up-Table "Eff 1 2 zone", and loss in the voltage inverter, which is determined by the constant value of its efficiency, taken at the level of 0.93.

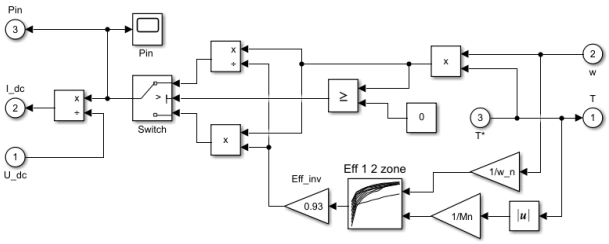


Fig. 13. **EMR model of the SPMSM**

***Source*: compiled by the authors**

The "Wheel" subsystem reflects the laws of transformation of the rotational motion of the wheel into the translational motion of the LEV according to the equations:

$$F_t = T / r_w \ , \quad \omega = V / r_w \ . \quad (39)$$

In EMR, the "Chassis" subsystem stores kinetic energy due to the mass of the EV. The input of this subsystem is the traction force on the wheel, which should provide the required speed. The second output will be the same speed value, and the second input will be the total force opposing the movement.

The operation of this subsystem is described by the differential equation

$$m \frac{dV}{dt} = F_t - F_{env} , \quad (40)$$

where $F_{env} = F_{roll} + F_{drag}$ is the total resistance force to motion, the components of which are determined by equations (2) and (3) and are formed in the "Environment" subsystem.

The control system blocks are marked in blue and placed parallel to the corresponding blocks of the modeled system.

The "Wheel inversion" block is built on clearly inverse mathematical expressions compare to the "Wheel" subsystem.

Since energy is stored in the "Chassis" subsystem, it is impossible to implement its direct inversion. For such subsystem, a separate closed loop must be created. In this case, it will be a proportional wheel speed controller, which is formed by the expression

$$F_t^* = K_V \left[V^*(t) - V(t) \right] + F_{env}(t) , \quad (41)$$

where K_V is the speed controller gain.

The "Strategy block" provides the transfer of the torque reference generated by the "Wheel inversion" block to the "SPMSM" subsystem, taking into account the permissible torque value, which is limited by the DC supply voltage.

The reference for the control system is formed by the "Drive Cycle Source" subsystem (not shown

ISSN 2663-0176 (Print)
ISSN 2663-7731 (Online)

in Fig. 12), similar to that shown in Fig. 3, where the time dependence of the driving speed V^* in the WLTC Class 1 drive cycle is given.

According to the EMR model shown in Fig. 12, a computer model of the LEV under study operating in the WLTC Class 1 drive cycle was built in the MATLAB/Simulink environment.

5.2. Results of the computer simulation of the LEV under study operation with experimental and typical SPMSMs

Computer simulation of two EMR models of the LEV under study movement in the WLTC Class 1 drive cycle, with experimental and typical SPMSMs, respectively, showed that the models correctly reproduce the specified angular velocity profile and the generated motor torque, similar to those shown in Fig. 4. Fig. 14 shows the main simulation result in the form of time diagrams of the change in the total energy consumed from the DC power source for the two studied cases, as well as separately the energy spent on traction and the energy returned to the power source because of regenerative braking.

Comparison of the obtained efficiency maps for the experimental (Fig. 11a) and typical (Fig. 11b) SPMSM shows that both designed electric machines provide zones of maximum efficiency in the ranges required for the LEV under study operating in the WLTC class 1 drive cycle. However, the experimental SPMSM is characterized by 1-2 % higher efficiency in the zone of its maximum. In addition, the zone of maximum torque limitation in the experimental SPMSM is significantly larger than one in the typical SPMSM, which is due to the FW. However, it is precisely due to the FW that the experimental motor has two times lower rated power.

6.DISCUSSION OF RESULTS

A separate important conclusion is that the value of the current component i_{d0} at maximum SPMSM efficiency, taking into account copper and iron losses, is practically independent of the load torque and is constant for a given angular velocity (Fig. 10a), both in the constant torque and FW regions. This feature simplifies the implementation of vector control of SPMSM.

The obtained time dependences of the total energy consumed by the electric drive of the LEV during movement in the drive cycle (Fig. 14a) show that in the case of using the experimental SPMSM with its speed regulation in two regions, with constant torque and constant power, the energy consumption per cycle is lower by 2.37 % compared to the case of using a typical SPMSM with single region of speed regulation with constant torque. At the same time, the amount of energy spent on the traction of the LEV is lower by 1.82 % (Fig. 14b), and the amount of energy returned to the DC source during regenerative braking of the motor is higher by 3.62 % (Fig. 14c) for the drive with the experimental SPMSM compared to the drive with a typical motor.

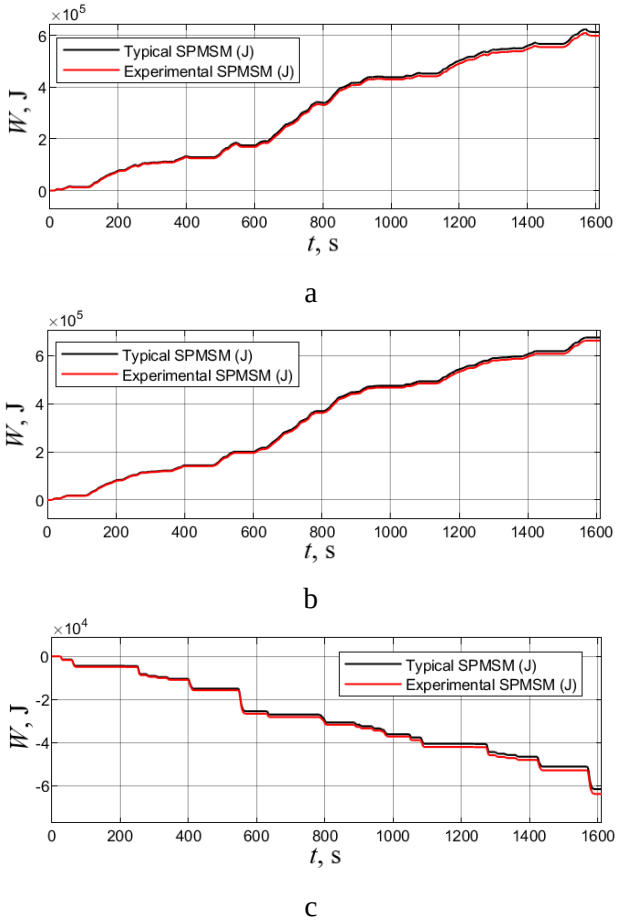


Fig. 14. **Time diagrams of DC power source energy variation during the LEV execution of the WLTC class 1 drive cycle for the two investigated SPMSMs:**
a – total energy consumed from the DC power source; b – energy expended on traction; c – energy returned to the power source at regenerative braking
***Source*: compiled by the authors**

The use of the obtained efficiency maps makes it possible to implement the model of the electric motor and its control system in a computer model built using the EMR method as simply as possible.

7. CONCLUSIONS

The conducted studies on determining the SPMSM parameters based on the needs of a specific

LEV operating in a specific drive cycle have confirmed the effectiveness of this approach. In particular, for the selected electric bicycle operating in the WLTC class 1 cycle, it is advisable to apply vector control of the motor speed in two regions: the constant torque and the constant power by means of FW. In this case, the choice of the FW control range at the value equal to two ensures good agreement of the ω-T range, in which the motor most often operates in the applied drive cycle, with the zone of maximum efficiency on the efficiency map obtained for the developed experimental SPMSM. Computer simulation of the electric bicycle operation in the WLTC class 1 drive cycle, implemented using the EMR method, showed slightly higher energy performance of the drive with the experimental SPMSM compared to the drive based on the typical SPMSM. However, the main advantage of the experimental motor over the traditional one is its half-smaller rated power, which is due to the two-region angular velocity control. This provides a significant reduction in the weight and dimensions of the drive in-wheel motor.

Further research will be aimed at implementing such a method of in-wheel SPMSM vector control, which will provide the required starting traction torque and will be based on simple rotor position sensors.

Conflict of interests: Authors declare that they do not have conflict of interests, in particular financial, personal, copyright or any of a different nature, which could have influenced the research, as well as the results published in this articles

Financing: Research was carried out without financial support

Accessibility data: All data available in digital or graphic form in the main text manuscript

Using artificial intelligence tools: Authors confirm that they did not use instrumental AI tools for writing this one work

REFERENCES

1. Gnanavendan, S., Selvaraj, S. K., Dev, S. J., Mahato, K. K., Swathish, R. S., Sundaramali, G., Accouche, O. & Azab, M. “Challenges, solutions and future trends in EV-Technology: A review”. *IEEE Access*. 2024; 12: 17242–17260, https://www.scopus.com/pages/publications/85182942442. DOI: https://doi.org/10.1109/ACCESS.2024.3353378.

2. Ewert, A., Brost, M., Eisenmann, C. & Stieler, S. “Small and light electric vehicles: An analysis of feasible transport impacts and opportunities for improved urban land use”. *Sustainability*. 2020; 12 (19): 8098, https://www.scopus.com/pages/publications/85092629550. DOI: https://doi.org/10.3390/su12198098.

3. Mesimäki, J. & Lehtonen, E. “Light electric vehicles: The views of users and non-users”. *European Transport Research Review*. 2023; 15 (1), https://www.scopus.com/pages/publications/85172356090. DOI: https://doi.org/10.1186/s12544-023-00611-3.

4. Voytenko, V. A., Vodichev, V. V., Kalinin, A. O. & Gladchenko, V. V. “Asynchronous traction electric drive for a cheap city passenger vehicle” (in Ukrainian). *Informatic. Culture. Technology*. 2025; 2: 485–495. DOI: https://doi.org/10.15276/ict.02.2025.73.

5. Li, L., Dai, L., Niu, S., Fu, W. & Chau, K. T. “Critical review of direct-drive in-wheel motors in electric vehicles”. *Energies*. 2025; 18 (6): 1521, https://www.scopus.com/pages/publications/105001096226. DOI: https://doi.org/10.3390/en18061521.

6. Pellegrino, G., Vagati, A., Boazzo, B. & Guglielmi, P. “Comparison of induction and PM synchronous motor drives for EV application including design examples”. *IEEE Transactions on Industry Applications*. 2012; 48 (6): 2322–2332. DOI: https://doi.org/10.1109/TIA.2012.2227092.

7. Mohanraj, D., Aruldavid, R., Verma, R., Sathiyasekar, K., Abdulwasa, B. B. & Chokkalingam, B. “A review of BLDC motor: State of art, advanced control techniques, and applications”. *IEEE Access*. 2022; 10: 54833–54869, https://www.scopus.com/pages/publications/85131708867.
DOI: https://doi.org/10.1109/ACCESS.2022.3175011.

8. Wang, J., Yuan, X. & Atallah, K. “design optimization of a surface-mounted permanent-magnet motor with concentrated windings for electric vehicle applications”. *IEEE Transactions on Vehicular Technology*. 2013; 62 (3): 1053–1064. DOI: https://doi.org/10.1109/TVT.2012.2227867.

9. Bianchi, N., Carlet, P. G., Cinti, L. & Ortombina, L. “A review about flux-weakening operating limits and control techniques for synchronous motor drives”. *Energies*. 2022; 15 (5): 1930. DOI: https://doi.org/10.3390/en15051930.

ISSN 2663-0176 (Print)
ISSN 2663-7731 (Online)

10. Alwaqfi, S., Alzayed, M. & Chaoui, H. “Flux-weakening control methods for permanent magnet synchronous machines in electric vehicles at high speed”. *Electronics*. 2025; 14 (19): 3779. DOI: https://doi.org/10.3390/electronics14193779.

11. Beshta, O. S., Beshta, O. O., Beshta, D., Tkachenko, S., Khalaimov, T. & Skliar, D. “Technologies for Increasing the energy efficiency of electric vehicles”. *2023 IEEE 5th International Conference Modern Electrical and Energy Systems (MEES)*. Kremenchuk, Ukraine. 2023. DOI: https://doi.org/10.1109/MEES61502.2023.10402470.

12. Roshandel, E., Mahmoudi, A., Kahourzade, S. & Soong, W. L. “Efficiency maps of electrical machines: A tutorial review”. *IEEE Transactions on Industry Applications*. 2023; 59 (2): 1263–1272, https://www.scopus.com/pages/publications/85139516509. DOI: https://doi.org/10.1109/TIA.2022.3210077.

13. Roshandel, E., Mahmoudi, A., Kahourzade, S., Yazdani, A. & Shafiullah, G. M. “Losses in efficiency maps of electric vehicles: An overview”. *Energies*. 2021; 14 (22): 7805, https://www.scopus.com/pages/publications/85119976837. DOI: https://doi.org/10.3390/en14227805.

14. Mellor, P. H., Wrobel, R. & Holliday, D. “A computationally efficient iron loss model for brushless AC machines that caters for rated flux and field weakened operation”. *2009 IEEE International Electric Machines and Drives Conference*. Miami, FL, USA. 2009. p. 490-494 DOI: https://doi.org/10.1109/IEMDC.2009.5075251.

15. Kahourzade, S., Mahmoudi, A., Soong, W. L., Ertugrul, N. & Pellegrino, G. “Estimation of PM machine efficiency maps from limited experimental data”. *2018 IEEE Energy Conversion Congress and Exposition (ECCE)*. Portland, OR, USA. 2018. p. 4315–4322. DOI: https://doi.org/10.1109/ECCE.2018.8557885.

16. Popescu, L. & Stănescu, A. “Efficiency maps for an EV BLDC motor using analytic calculation and simulation”. *APME: Electric Machines, Materials and Drives – Present and Trends*. 2022; 18 (1): 89–99. DOI: https://www.doi.org/10.36801/apme.2022.1.11.

17. Song, L., Li, Z., Cui, Z. & Yang, G. “Efficiency map calculation for surface-mounted permanent-magnet in-wheel motor based on design parameters and control strategy”. *2014 IEEE Conference and Expo Transportation Electrification Asia-Pacific (ITEC Asia-Pacific)*. Beijing, China. 2014. p. 1–6. DOI: https://doi.org/10.1109/ITEC-AP.2014.6940816.

18. Li, Z. & Miotto, A. “Concentrated-winding fractional-slot synchronous surface PM motor design based on efficiency map for in-wheel application of electric vehicle”. *Proceedings of 2011 IEEE Vehicle Power and Propulsion Conference*. Chicago, IL, USA. 2011. p. 1-8. DOI: https://doi.org/10.1109/VPPC.2011.6043087.

19. Toda, H., Xia, Z. P., Wang, J., Atallah, K. & Howe, D. “Rotor eddy-current loss in permanent magnet brushless machines”. *IEEE Transactions on Magnetics*. 2004; 40 (4): 2104–2106. DOI: https://doi.org/10.1109/TMAG.2004.832481.

20. Kiyota, K., Sugimoto, H. & Chiba, A. “Comparison of energy consumption of SRM and IPMSM in automotive driving schedules”. *2012 IEEE Energy Conversion Congress and Exposition (ECCE)*. Raleigh, NC, USA. 2012. p. 853–860. DOI: https://doi.org/10.1109/ECCE.2012.6342729.

21. “Emission test cycles: WLTC”. *DieselNet*. – Available from: https://dieselnet.com/standards/cycles/wltp.php. – [Accessed: 13, August 2026].

22. “Electric bicycle M20-III 2000W 36Ah electric fatbike with extended range”. *Dobramama*. 2026. – Available from: https://dobramama.com.ua/10049-elektrovelosyped-m20-iii-2000w-36ah-elektrofetbajk-z-velykym-zapasom-hodu. – [Accessed: 10, August 2026].

23. “WLTP-DHC-12-07e.xls”. *UNECE*. – Available from: https://www.unece.org/fileadmin/DAM/trans/doc/2012/wp29grpe/WLTP-DHC-12-07e.xls. – [Accessed: 10, August 2026].

24. Mahmoudi, A., Soong, W. L., Pellegrino, G. & Armando, E. “Efficiency maps of electrical machines”. *2015 IEEE Energy Conversion Congress and Exposition (ECCE)*. Montreal, QC, Canada. 2015. p. 2791–2799. DOI: https://doi.org/10.1109/ECCE.2015.7310051.

25. Shchur, I., Rusek, A. & Mandzyuk, M. “Power effective work of PMSM in electric vehicles at the account of magnetic saturation and iron losses”. *Przeglad Elektrotechniczny*. 2015; 91 (1): 199–202, https://www.scopus.com/pages/publications/84920455763. DOI: https://doi.org/10.15199/48.2015.01.45.

26. Shchur, I., Biletskyi, Y. & Kopchak, B. “Efficiency analysis and optimization of two-speed-region operation of permanent magnet synchronous motor taking into account iron loss based on linear non-equilibrium thermodynamics”. *Machines*. 2024; 12 (11): 826, https://www.scopus.com/pages/publications/85210164899. DOI: https://doi.org/10.3390/machines12110826.

27. Fernandez-Bernal, F., Garcia-Cerrada, A. & Faure, R. “Determination of parameters in interior permanent-magnet synchronous motors with iron losses without torque measurement”. *IEEE Transactions on Industry Applications*. 2001; 37 (5): 1265–1272. DOI: https://doi.org/10.1109/28.952501.

28. Chen, K., Bouscayrol, A., Berthon, A., Delarue, P., Hissel, D. & Trigui, R. “Global Modeling of Different Vehicles Using Energetic Macroscopic Representation”. *Proceedings of the 2008 IEEE Vehicle Power and Propulsion Conference (VPPC)*. Harbin, China. 2008. p. 533–539. DOI: https://doi.org/10.1109/VPPC.2008.4677728.

29. Shchur, I. Z. & Kovtun, V. O. “Control optimization of automatic multistage transmission in city electric bus”. *Applied Aspects of Information Technology*. 2022; 5 (2): 120–135. DOI: https://aait.op.edu.ua/?fetch=articles&with=info&id=115.

Received 03.09.2026
Received after revision 26.10.2026
Accepted 30.10.2026-

DOI: https://doi.org/10.15276/hait.09.2026.44
УДК 629.113.65:621.313.3:519.87.004

Розроблення внутрішньоколісного двигуна з розміщеними на поверхні ротора постійними магнітами для легкого електричного транспортного засобу на основі циклу WLTC класу 1

Щур Ігор Зенонович[1)]
ORCID: https://orcid.org/0000-0001-7346-1463; ihor.z.shchur@lpnu.ua. Scopus Author ID: 36348908300
Лутчин Ігор Юрійович[1)]
ORCID: https://orcid.org/0009-0003-2691-9381; ihor.y.lutchyn@lpnu.ua. Scopus Author ID: 60560224000
Ліс Марек[2)]
ORCID: https://orcid.org/0000-0001-5191-8303; marek.lis@pcz.pl. Scopus Author ID: 54415858000
[1)] Національний університет «Львівська політехніка», вул. Степана Бандери, 12. Львів, Україна
[2)] Політехніка Ченстоховська, Алея Армії Крайової 17. Ченстохова, Польща

АНОТАЦІЯ

Актуальність: Під час проєктування тягових електродвигунів традиційно домінує підхід, зорієнтований на роботу двигуна в точці номінального режиму. Однак, двигуни електричних транспортних засобів постійно працюють у широкому діапазоні зміни моменту та кутової швидкості. Відповідно доцільно проєктувати електричну машину так, щоб зона її оптимальної роботи (максимальної енергетичної ефективності) знаходилася в області, де двигун працює найбільше часу в транспортному циклі. Огляд літератури показує, що такий підхід дає змогу підвищити енергетичну ефективність роботи тягового двигуна, а разом і з ним загальну ефективність системи електропривода. **Метою статті** є розроблення тягового синхронного двигуна з розміщеними на поверхні ротора постійними магнітами (SPMSM), вмонтованого в колесо дослідного легкого електричного транспортного засобу (ЛЕТЗ), швидкісного електровелосипеда, для ефективного відпрацювання ним нового транспортного циклу для ЛЕТЗ – WLTC класу 1. **Методи**: Для досягнення поставленої мети отримано гістограму поєднання кутової швидкості і моменту під час роботи дослідного ЛЕТЗ за відпрацювання ним вказаного транспортного циклу. Відповідно до визначеного з гістограми діапазону, де привод працює найчастіше, визначено параметри експериментального SPMSM, причому за його роботи в двох зонах регулювання кутової швидкості – зі сталим моментом та зі сталою потужністю. В середовищі MATLAB/Simulink побудовано модель SPMSM з врахуванням втрат в міді і сталі, на якій досліджено енергетичну ефективність роботи експериментального (з двозонним регулюванням швидкості) і типового (з однозонним регулюванням) SPMSM у всьому моментно-швидкісному діапазоні роботи, на підставі чого в середовищі Surfer побудовано карти їх енергетичної ефективності. Порівняння ефективності роботи дослідного ЛЕТЗ в транспортному циклі з експериментальним і типовим двигунами було проведено шляхом моделювання в середовищі MATLAB/Simulink за методом Energetic Macroscopic Representation (EMR). **Результати дослідження** показали зменшення витрат електроенергії на

відпрацювання транспортного циклу лослідним ЛЕТЗ з експериментальним SPMSM на 2,37 %, а також приріст енергії рекуперативного гальмування на 3,62 % у порівнянні із типовим двигуном. **Висновки**: SPMSM із двозонним регулюванням кутової швидкості та відповідно отриманими параметрами дає змогу знизити вдвічі його номінальну потужність та одночасно підвищити загальну енергетичну ефективність роботи системи привода електровелосипеда.

Ключові слова: легкий електричний транспортний засіб; транспортний цикл WLTC class 1; синхронний двигун з постійними магнітами; двозонне регулювання швидкості; карта енергетичної ефективності; Energetic Macroscopic Representation (EMR)

ABOUT THE AUTHORS



Ihor Shchur – Doctor of Engineering Sciences, Professor, Head of the Department of Electromechanical and Electrical Systems. Lviv Polytechnic National University. 12, Stepana Bandery Str. Lviv, 79013, Ukraine
ORCID: https://orcid.org/0000-0001-7346-1463; ihor.z.shchur@lpnu.ua. Scopus Author ID: 36348908300
***Research field*:** Direct drives based on synchronous machines with permanent magnets; Electric drives and control systems for electric vehicles; Small power renewable energy conversion systems, including photovoltaic and wind turbine; Hybrid energy storage systems including batteries and supercapacitors; Energy-based mathematical modeling of multi-physics systems; Passivity-based controlled systems

Щур Ігор Зенонович - доктор технічних наук, професор, завідувач кафедри Електромеханічних та електротехнічних систем. Національний університет «Львівська політехніка», вул. Степана Бандери, 12. Львів, 79013, Україна
***Галузь досліджень*:** Прямі приводи на основі синхронних машин із постійними магнітами; електроприводи та системи керування для електротранспорту; системи перетворення енергії відновлюваних джерел малої потужності, зокрема фотоелектричні та вітроенергетичні установки; гібридні системи накопичення енергії, що включають акумулятори та суперконденсатори; математичне моделювання мультифізичних систем на основі енергетичного підходу; системи керування, що ґрунтуються на властивості пасивності



Ihor Lutchyn – PhD student, Department of Electromechanical and Electrical Systems. Lviv Polytechnic National University. 12, Stepana Bandery Str. Lviv, 79013, Ukraine
ORCID: https://orcid.org/0009-0003-2691-9381; ihor.y.lutchyn@lpnu.ua. Scopus Author ID: 60560224000
***Research field*:** Hardware-In-The-Loop (HIL) systems; Regenerative braking of BLDC motors in the light electric vehicles; Efficient control of permanent magnet traction motors

Лутчин Ігор Юрійович - аспірант кафедри Електромеханічних та електротехнічних систем. Національний університет «Львівська політехніка», вул. Степана Бандери, 12. Львів, 79013, Україна
***Галузь досліджень*:** Системи з апаратною складовою в контурі керування (HIL); рекуперативне гальмування безщіткових двигунів постійного струму (BLDC) у легких електричних транспортних засобах; ефективне керування тяговими двигунами з постійними магнітами



Marek Lis - Doctor of Engineering Sciences, Dean of the Faculty of Electrical Engineering. Częstochowa University of Technology. 17, Al. Armii Krajowej, Częstochowa, 42-200, Poland
ORCID: https://orcid.org/0000-0001-5191-8303; marek.lis@pcz.pl. Scopus Author ID: 54415858000
***Research field*:** Design and modeling of electric machines and drives, in particular machines used in metallurgical processes (roller table drives). Participated in several designs and carried out a number of expertise reports in this field for industry, eg. Częstochowa Steelworks, Petroeltech Płock

Lis Marek - доктор технічних наук, професор, декан Електротехнічного факультету Політехніки Ченстоховської. Ченстохова, 42-200, Польща
***Галузь досліджень*:** Проектування та моделювання електричних машин та приводів, зокрема машин, що використовуються в металургійних процесах (приводи роликових столів). Брав участь у кількох проектних роботах та виконав низку експертних звітів у цій галузі для промисловості, наприклад, Ченстоховський сталеливарний завод, Петроелтех Плоцьк